CSCE Annual Conference

Growing with youth – Croître avec les jeunes

Laval (Greater Montreal)

June 12 - 15, 2019

BEARING CAPACITY ANALYSIS OF A SHALLOW FOUNDATION ON SOFT CLAY CONSIDERING VISCOPLASTIC BEHAVIOR

Luo, Y.[1,2] & Li, B.[1]

1 Department of Building, Civil and Environmental Engineering, Concordia University, Montreal, Quebec, Canada

2 ywluo1994@gmail.com

Abstract: The stress–strain behavior of soft clay soil is dependent on the applied strain rate and such time dependency behavior should be considered in geotechnical engineering projects such as the bearing capacity analysis for a foundation. Most previous studies focus on elastic-viscoplastic behavior of clay soil under an undrained stress path condition. The developed constitutive models cannot simulate the strong time dependent stress-strain relation of soft clay under drained stress path condition. In the long-term bearing capacity analysis for a shallow foundation, the neglect of the time dependent stress-strain relation of soft clay may result in inaccurate result. In this study, finite element modeling on long-term bearing capacity of a shallow foundation on soft clay is performed. The strain-rate-dependent soil behavior is modeled using the Drucker-Prager/Cap model with the consideration of soil creep behavior. Both consolidation creep and shear creep mechanisms are considered in the modeling. The result shows that the considering of viscoplastic behavior of clay soils does not affect the ultimate bearing capacity. However, it yields the lower bound of developed shear stress of a shallow foundation at a given vertical displacement, which is to be conservative from the engineering point of view.

1 INTRODUCTION

As the population increases, people tend to build on soft clay deposits which was previously treated unsuitable for residential housing and construction projects (Fang 2013). The mechanical behavior of soft clay soil is highly dependent on the applied stress path and strain rate, which makes soft clay soils display strong viscoplastic behavior (Fodil et al. 1998, Yin and Graham 1999, Yin et al. 2011). An accurate characterization of the complex shear and consolidation behavior of clay soil is critical for a foundation's bearing capacity analysis (Taiebat and Carter 2000). Most previous studies focus on elastic-viscoplastic behavior of clay soil under an undrained stress path condition (Yin and Graham 1999, Yin et al. 2010, Yin et al. 2011). The developed constitutive models cannot simulate the strong time dependent stress-strain relation of soft clay under the drained stress path condition. In the long-term bearing capacity analysis for a shallow foundation, the neglect of the time dependent stress-strain relation of soft clay may result in inaccurate result. In this study, we performed finite element modeling on the bearing capacity of a shallow foundation on soft clay using Drucker-Prager/Cap model combined with Singh-Mitchell creep model, where the drained creep behavior is considered.

2 ELASTIC-VISCOPLASTIC BEHAVIOR OF CLAY SOIL

Under a drained stress path condition, the total stain for a soft clay is given by

[1] $d\varepsilon = d\varepsilon^e + d\varepsilon^p + d\varepsilon^{cr}$

where $d\varepsilon^e$ is the elastic strain, $d\varepsilon^p$ is the time-independent plastic strain, and $d\varepsilon^{cr}$ is the creep strain. In this study, the time-independent plastic strain is characterized by the Drucker-Prager/Cap model and the creep strain is characterized by the Singh-Mitchell creep model.

2.1 Drucker-Prager/Cap model

The Drucker – Prager/cap plasticity model has been widely used in the numerical analysis of geotechnical problems due to its capable of considering the effect of stress history, stress path and the combined shear-consolidation yielding behavior in clay soils (Helwany 2007). The yield surface of the modified Drucker – Prager/cap plasticity model consists of three parts: a Drucker-Prager shear failure surface, an elliptical *cap* and a transition region between the shear failure surface and the cap. If we neglect the transition region between the shear failure surface and the cap, the yield surface is displayed in Figure 1.

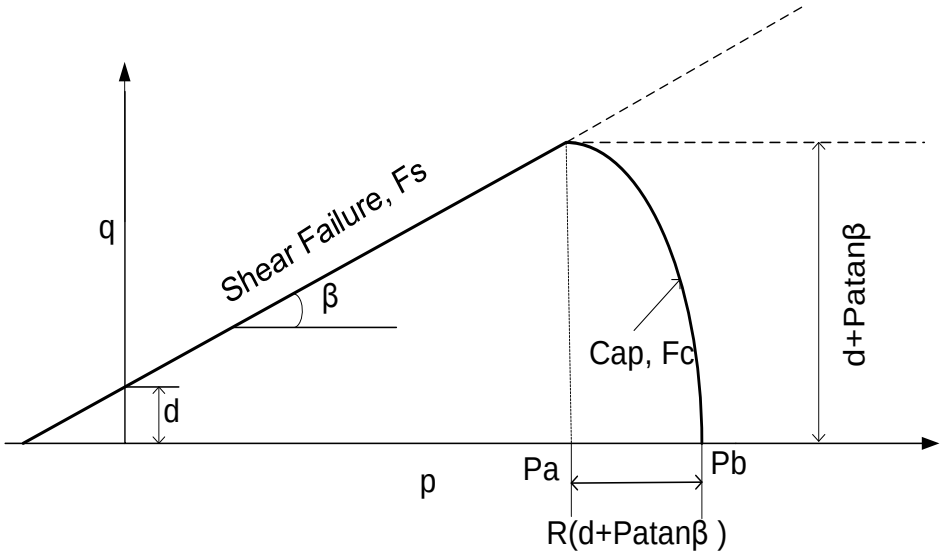

Figure 1 Yield surfaces of the modified cap model in the meridional (p–q) plane, modified after Abaqus (2016).

The Drucker-Prager failure surface and the cap yield surface determine the shear and consolidation yielding, respectively. The Drucker-Prager failure surface is given by Equation [2],

[2] $f_s^p = q - p\tan\beta - d$

where p is the effective mean stress, which can be defined by the effective stress tensor σ as: $p = \frac{1}{3}trace(\sigma)$; q is the Mises equivalent stress, which can be defined by the deviatoric stress tensor as: $q = \sqrt{\frac{3}{2}\mathbf{S}:\mathbf{S}}$, where $\mathbf{S}$ is the deviatoric stress tensor defined as $\mathbf{S} = \boldsymbol{\sigma} - p\mathbf{I}$ and $\mathbf{I}$ is the unit matrix; β and d are the friction angle and cohesion in p-q space, respectively;

When the stress state causes yielding on the Drucker – Prager shear failure surface, the soil is treated as perfect plastic material where shear hardening is not considered in this study.

The cap yield surface is an ellipse（with an eccentricity R） in the $p-q$ plane. The cap surface hardens or softens can be considered as a function of the volumetric plastic strain. The cap yield surface is given as

[3] $f_c^p = \sqrt{\left(p - p_a\right)^2 + \left(Rq\right)^2} - R(d + p_a \tan\beta)$

Where R is a material parameter which controls the shape of the cap, and p_a is an evolution parameter which controls the hardening – softening behavior as a function of the volumetric plastic strain. The relation the mean effective (yield) stress p_b and the volumetric plastic strain can be described by a nonlinear function to characterize the hardening-softening behavior.

In the Drucker-Prager/Cap model, the flow potential surface in the $p-q$ plane consists of two parts (Figure 2).

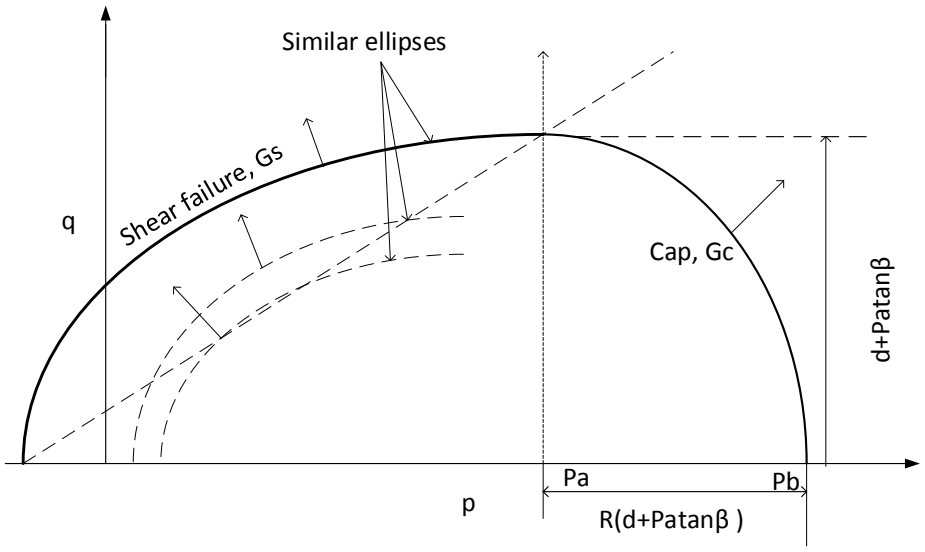

Figure 2 Flow potentials of the modified cap model in the p–q plane, modified after Abaqus (2016).

The plastic flow is defined by a flow potential which is identical to the yield surface (i.e., associated flow) in the cap region. A non-associated flow is assumed for the Drucker – Prager failure surface: as shown in Figure 2, the shape of the flow potential in the $p-q$ plane is different from the yield surface.

In the Drucker – Prager failure and transition regions, the elliptical flow potential surface portion is given as

[4] $g_s^p = \sqrt{\left[\left(p_a - p\right)\tan\beta\right]^2 + q^2}$

The elliptical flow potential surface in the cap region is given as

[5] $g_c^p = \sqrt{\left(p - p_a\right)^2 + R^2 q^2}$

2.2 Singh-Mitchell creep model

For the Drucker-Prager/Cap model with the Singh-Mitchell model, there are two separate and independent creep mechanisms. One is shear creep which is attributed to the cohesion mechanism ($d\varepsilon_s^{cr}$), and the other is consolidation creep which is attributed to consolidation mechanism ($d\varepsilon_c^{cr}$). The total creep strain is a combination of those two components:

[6] $$d\varepsilon^{cr} = d\varepsilon_s^{cr} + d\varepsilon_c^{cr}$$

The regions of activity of shear and consolidation creep mechanisms are illustrated in Figure 3. The shear mechanism is active for all stress states which have a positive equivalent creep stress. The consolidation mechanism is active for all stress states where the pressure is larger than p_a. It can be noticed that there is a region where both creeps can occur (Figure 3).

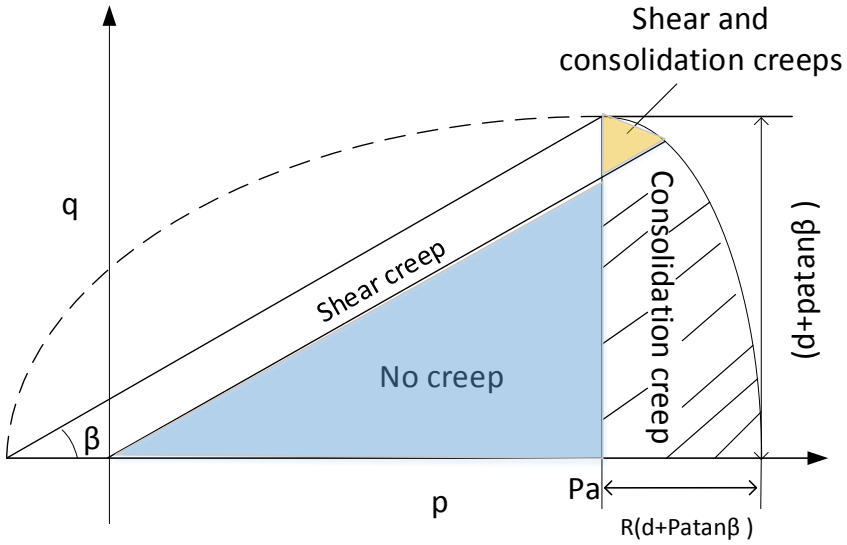

Figure 3 Regions of activity of shear and consolidation creep mechanisms, modified after Abaqus (2016).

The creep potential functions for both mechanisms are given in Equations [7] and [8], respectively.

[7] $$g_s^{cr} = \sqrt{\left(0.1\frac{d}{(1-\frac{1}{3}\tan\beta)}\tan\beta\right)^2 + q^2} - p\tan\beta$$

[8] $$g_c^{cr} = \sqrt{(p-p_a)^2 + R^2q^2}$$

The Singh-Mitchell creep model for shear creep takes the form as:

[9] $$\dot{\varepsilon}_{11} = A^s e^{\alpha^s \sigma_{cr}^s}\left(\frac{t_1}{t}\right)^{m^s}$$

For shear creep, the equivalent creep stress, σ_{cr}^{s} is determined as the intersection of the equivalent creep surface with the uniaxial compression curve. A^{s}, α^{s}, and m^{s} are three creep parameters which should be derived from creep or relaxation tests results.

[10] $$\sigma_{cr}^{s} = \frac{q - p\tan\beta}{\left(1 - \frac{1}{3}\tan\beta\right)}$$

The Singh-Mitchell creep model for consolidation creep takes the form as:

[11] $$\dot{\varepsilon}_{v} = A^{c} e^{\alpha^{c}\sigma_{cr}^{c}} \left(\frac{t_1}{t}\right)^{m^{c}}$$

For consolidation creep, σ_{cr}^{c} is derived from the mean stress p,

[12] $$\sigma_{cr}^{c} = p - p_{a}$$

According to the experimental results of Hewage (2018), we obtained the constitutive parameters of a soft clay soil (Regina clay, Canada). The parameters are listed in Table 1, and they will be used for the subsequent numerical modeling analysis.

Table 1 Material properties for constitutive modeling on Regina clay

Parameter	Elastic		Cap plasticity				Strain hardening				
	E (MPa)	ν	d (kPa)	β (deg)	R	Initial yield	K	e_0	λ	k	p_0 (kPa)
Value	15	0.3	60	42	0.3	0	1	0.93	0.2	0.03	58

Parameter	Consolidation creep				Shear creep			
	A^c	α^c(1/kPa)	m^c	t_1	A^s	α^s(1/kPa)	m^s	t_1
Value	0.000115	0.023458	0.929771	1	0.000118	0.07	0.625374	1

3 NUMERICAL MODELING OF BEARING CAPACITY ANALYSIS

With the above-mentioned soil models and the corresponding constitutive parameters of the Regina clay soil, we were able to perform a numerical analysis of the stability of layers of Regina clay soil which was loaded by a rigid footing. The simulation was conducted using Abaqus 6.14 where the finite element method was applied, and the problem was treated in 2D plane strain condition. Shown in Figure 4, the modeled Regina clay soil formation is 10 m in deep and 10 m in width. The shallow foundation is a 1-m-thick rigid and perfectly rough plate that spans a 1m on the top-left side of soil layers. The soil formation was divided into 15 layers from the top to the bottom, which corresponds to the different hydrostatic compression yield stress (pre-consolidation stress). The hydrostatic compression yield stress in the top 3 m is the same (58 kPa), and this pre-consolidation stress increases with an increase of buried depth below 3 m. The strip foundation is assumed to be in perfect contact with the soil, which means that

relative displacement between the foundation and soil is not permitted. Reduced-integration bilinear plane strain quadrilateral elements are used for the soil. The mesh is set finer in the vicinity of the foundation because as this zone bears most of the stress concentration (Figure 4). Twenty elements haven been averagely applied on the 1m footing part, and 40 elements haven been applied with an increase element size on the other 9m of top surface. The element size increases gradually with an increase of buried depth in the top 3 meters, and the other element size keeps the same in the depth below 3m. Two monitoring points (P1 and P2) were selected for tracking the stress paths. For the boundary conditions, the base of the soil layer is fixed in both the horizontal and vertical directions. The right and left vertical boundaries are fixed in the horizontal direction but free in the vertical direction. In the beginning of the analysis (static, general step), a surcharge load with a pressure of 57 kPa was applied to the top surface of soil layer and a gravity load was applied to the whole soil body. Pore water pressured was not considered in this study since we are focusing on the mechanical behavior under the drained stress path condition.

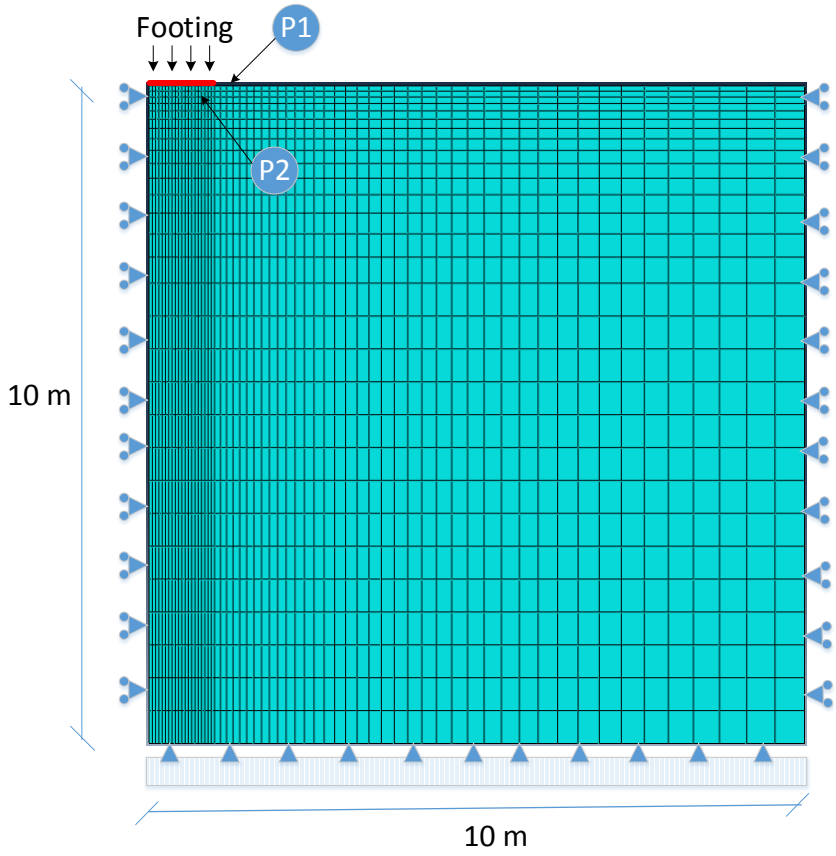

Figure 4 Sketch showing the configuration, mesh, and two monitoring points of the studied problem.

After the completion of surcharge and gravity loads, a displacement of 0.85 m is applied on the 1m wide foundation part using different time intervals (1 day, 30 days, and 60days) in visco step. The different boundary condition applied to the top surface of foundation causes different bearing capacity-displacement results (Figure 5).

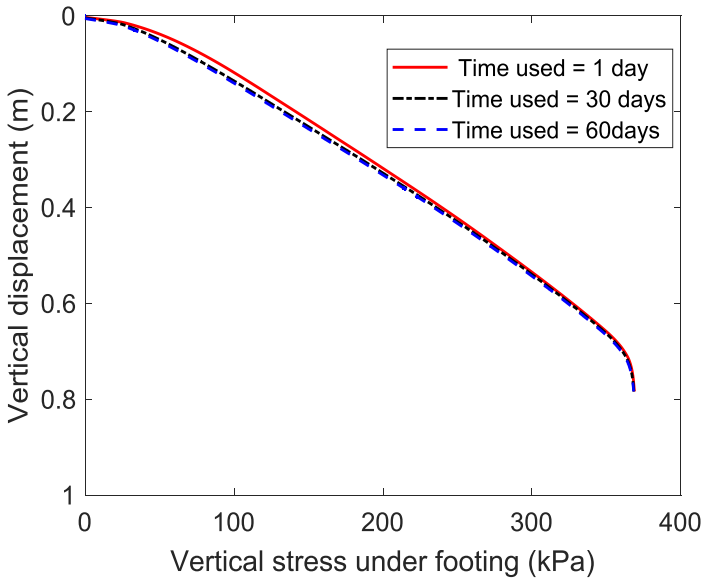

Figure 5 Modeled load-displacement curve for the studied footing problem using different time intervals.

The results display that there is no difference in the ultimate bearing capacity (368 kPa) for those cases using different strain rates. However, the vertical stress for the case with more creep behavior (30 days and 60 days) is always lower than the case with less creep (1 day). At a given vertical displacement, for instance 0.2 m, the developed vertical stress for the one with a lower strain rate (60 days) gets 10 kPa less than the one with a higher strain rate (1 day). A comparison of the modeled Mises stress distributions in Regina clay soil subjected to strain rates is displayed in Figure 6. A slightly lower value of Mises stress can be found for the case with a lower strain rate (60 days). Similar situation is noticed for the volumetric inelastic strain in Regina clay (Figure 7), where the one with a lower strain rate (60 days) displays less volumetric plastic strain.

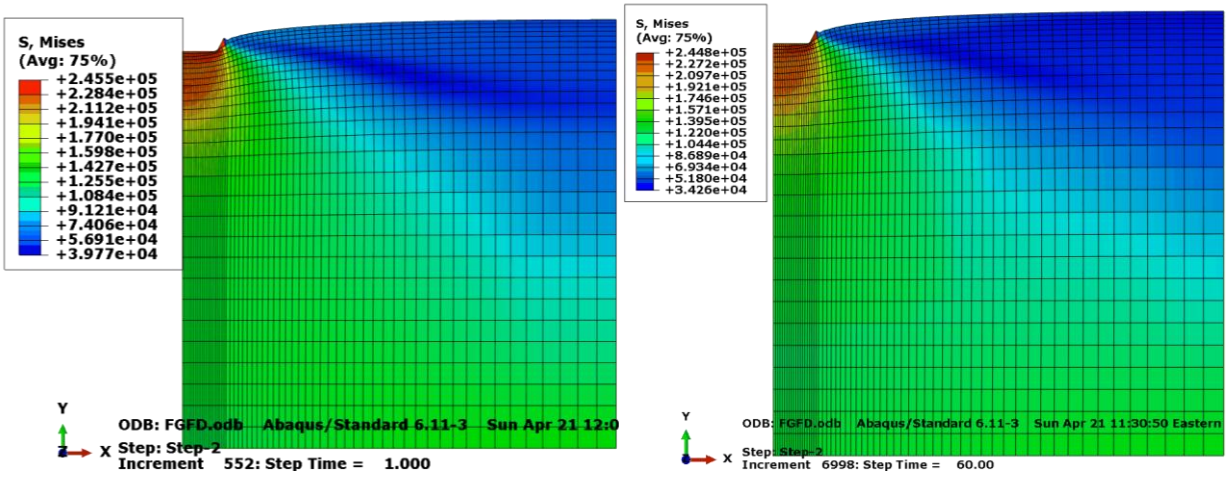

(a) (b)

Figure 6 Modeled Mises stress (in Pa) distributions in Regina clay soil using (a) one day and (b) 60 days.

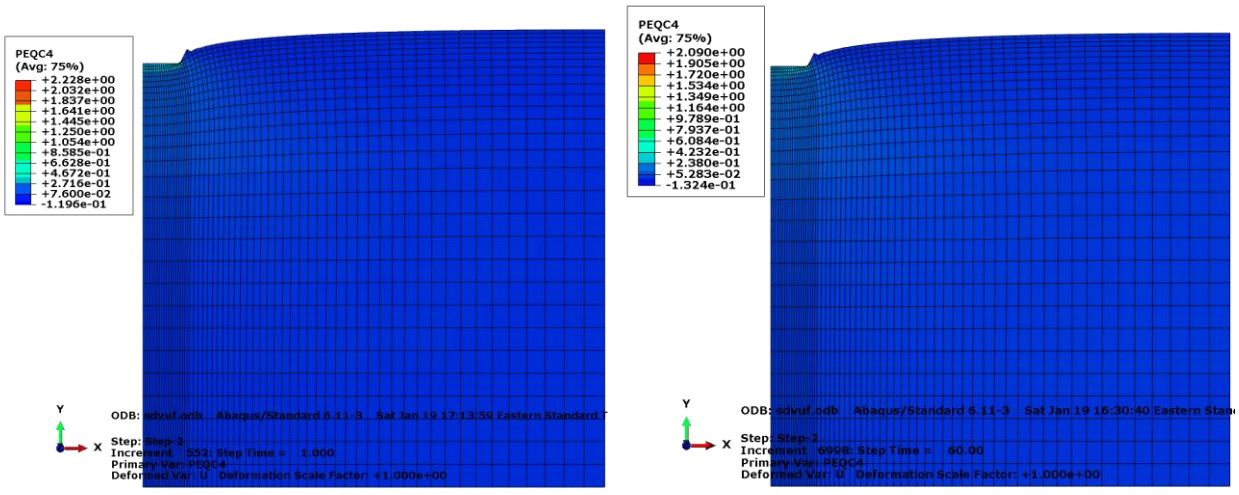

(a) (b)

Figure 7 Modeled total volumetric inelastic strain in Regina clay soil using (a) one day and (b) 60 days (PEQC4 stands for volumetric inelastic strain in Abaqus).

A plot of the stress paths of two monitoring points can be found in Figure 8. The curve shows that the generated creep behavior (for the cases with longer time intervals) affects the generation of shear stress. However, they attain the same ultimate shear stress when soil gets failure.

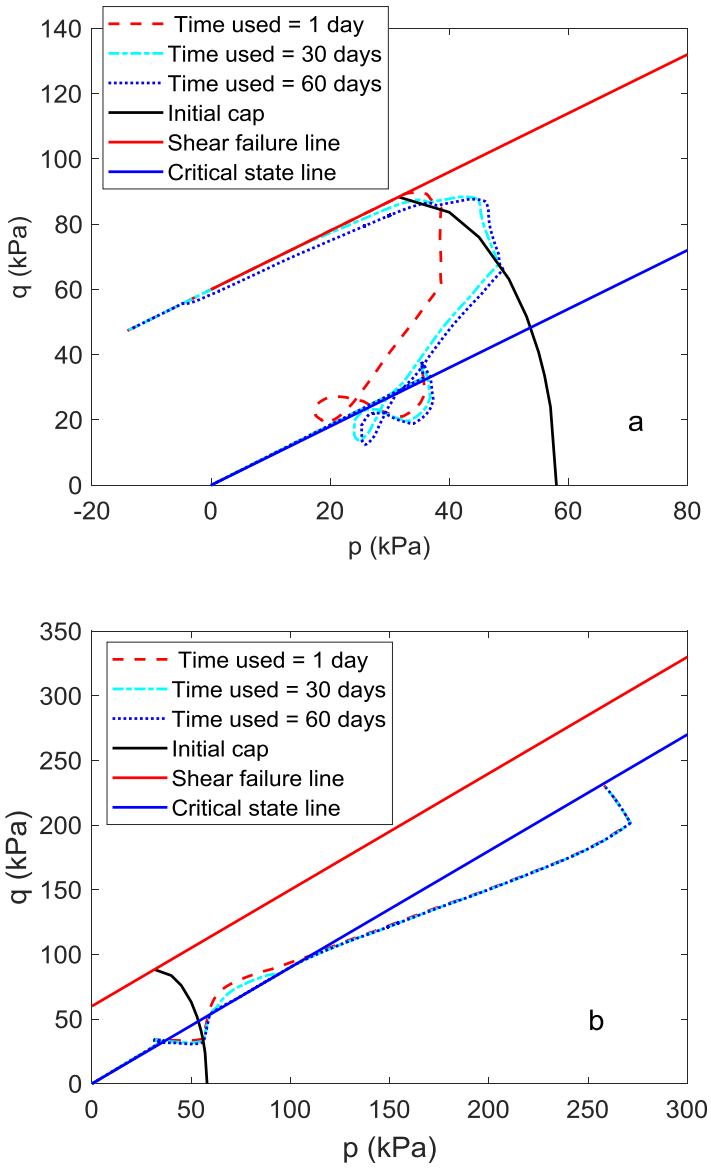

Figure 8 Modeled stress paths of (a) monitoring point 1 and (b) monitoring point 2 in p–q space.

4 SUMMARY

The strain-rate-dependent soil behavior can be modeled using the Drucker-Prager/Cap model with the consideration of soil creep behavior. Both shear creep and consolidation creep mechanisms can be considered in the modeling. A numerical analysis of the bearing capacity of a shallow foundation on Regina clay soil shows that the considering of viscoplastic behavior of clay soils does not affect the ultimate bearing capacity. However, considering viscoplastic behavior of clay soils yields the lower bound of developed shear stress of a shallow foundation, which is to be conservative from the engineering point of view. It is recommended to apply such viscoplastic model to simulate geotechnical issues where shear plastic strain plays a major role for the factor of safety (e.g., slope stability analysis).

ACKNOWLEDGEMENTS

The authors would like to acknowledge the support by NSERC Discovery Grant Canada (NO. RGPIN-2017-05169). The support by Dr. Rajitha Hewage and Prof. Ron Wong from the University of Calgary is also acknowledged.

REFERENCE

Abaqus. Abaqus theory manual, Simulia, 2016.

Fang, H.-Y. 2013. *Foundation engineering handbook.* Springer Science & Business Media.

Fodil, A., Aloulou, W., and Hicher, P. 1998. Viscoplastic behaviour of soft clay. *Pre-failure deformation behaviour of geomaterials:* 195.

Helwany, S. 2007*. Applied soil mechanics with ABAQUS applications*. John Wiley & Sons.

Hewage, R.E. 2018. An experimental study on time-dependent behaviour of reconstituted clayey soils in 1D and triaxial compression. *PhD thesis*, The University of Calgary, Alberta, Canada.

Taiebat, H., and Carter, J. 2000. Numerical studies of the bearing capacity of shallow foundations on cohesive soil subjected to combined loading. *Géotechnique*, **50**(4): 409-418.

Yin, J.-H., and Graham, J. 1999. Elastic viscoplastic modelling of the time-dependent stress-strain behaviour of soils. *Canadian Geotechnical Journal*, **36**(4): 736-745.

Yin, Z.-Y., Chang, C.S., Karstunen, M., and Hicher, P.-Y. 2010. An anisotropic elastic–viscoplastic model for soft clays. *International Journal of Solids and Structures* **47**(5): 665-677. doi: http://dx.doi.org/10.1016/j.ijsolstr.2009.11.004.

Yin, Z.-Y., Karstunen, M., Chang, C.S., Koskinen, M., and Lojander, M. 2011. Modeling time-dependent behavior of soft sensitive clay. *Journal of geotechnical and geoenvironmental engineering*, **137**(11): 1103-1113.